*Acta Oceanol. Sin.*, 2022, Vol. 41, No. 9, P. 1–18
https://doi.org/10.1007/s13131-022-1995-3
http://www.aosocean.com
E-mail: ocean2@hyxb.org.cn

# On the role of wave breaking in ocean dynamics under typhoon Matsa in the Bohai Sea, China

Menghan Wang[1†], Zengan Deng[1, 2*†]

[1] School of Marine Science and Technology, Tianjin University, Tianjin 300072, China

[2] Guangxi Key Laboratory of Marine Environment Change and Disaster in Beibu Gulf, Qinzhou 535011, China

Received 8 July 2021; accepted 29 November 2021

© Chinese Society for Oceanography and Springer-Verlag GmbH Germany, part of Springer Nature 2022

**Abstract**

The role of wave breaking (WB) in the ocean dynamics in the Bohai Sea, China under typhoon condition is systematically investigated utilizing a coupled wave-current model. The influences of WB on ocean dynamics and processes (mixing coefficient, temperature, mixed layer depth, and current) during the entire typhoon period (including the pre-typhoon, during-typhoon and after-typhoon stages) are comprehensively detected and discussed. Experimental results show that WB greatly enhances the turbulent mixing at about top 10 m depth under typhoon condition, the increase can be up to 10 times that of the normal weather. At the same time, WB generally strengthens the sea surface cooling by ~1.2°C at the during-typhoon stage, about 3 times that in normal weather. The mixed layer depth, is rapidly increased by ~1.6–3.6 m during typhoon due to WB, particularly, the deepening is stronger in the region from 120.5°E to 121.0°E on account of close to the typhoon eye. In addition, WB renders the current speed more uniformly within the entire depth in the Bohai Sea, the change in speed is ~0.2 m/s, whereas the alternation in current vector is generally opposite to the wind direction except for the typhoon eye region, reflecting that WB has an inhibitory effect on the typhoon-forced current change. The effects of WB on vertical mixing coefficient response to the typhoon rapidly, while the impacts of WB on temperature, and mixed layer depth present hysteretic responses to typhoon. Finally, the mechanisms and distribution characteristics of WB-induced mixing and tidal mixing are compared under typhoon condition.

**Key words:** wave breaking, tidal mixing, turbulent mixing, typhoon, coupled model

**Citation:** Wang Menghan, Deng Zengan. 2022. On the role of wave breaking in ocean dynamics under typhoon Matsa in the Bohai Sea, China. Acta Oceanologica Sinica, 41(9): 1–18, doi: 10.1007/s13131-022-1995-3

## 1 Introduction

Both winds and tides are the major mechanical energy driving the turbulent mixing, of which winds are mainly acting on the sea surface (Wunsch and Ferrari, 2004), while the mixing near the bottom is predominantly controlled by tides (Meng et al., 2020). In the upper ocean, in addition to turbulence generated by wind-driven currents, wave breaking (WB) can also produce an enormous amount of turbulent kinetic energy (TKE) injecting downward into the ocean. The momentum of the wind is first transferred to the waves and then to the currents mainly through the action of WB (Phillips, 1977). This process significantly enhances the TKE near the surface (Drennan et al., 1992; Yang et al., 2003). About half of WB-generated TKE dissipates within the depth of significant wave height ($H_s$), and the remaining continues to transmit downward, which will affect the vertical distribution of the upper ocean temperature and circulation (Feddersen, 2012). The overall effect depth can reach several times of the $H_s$ (Agrawal et al., 1992; Scully et al., 2016; Sun et al., 2006; Gerbi et al., 2009). The observations of the wave breaking zones that are mainly controlled by the tides and winds demonstrate that the turbulence generated by WB is critically important to estimate the vertical structure of the water column in shallow water areas (Zippel et al., 2018). On account of the shallow water depth and the complex terrain in the Bohai Sea (BS), both WB and tidal mixing play significant roles in BS dynamic processes (Jones and Monismith., 2008; Zhao et al., 2019). Therefore, the characteristics and distribution patterns of WB induced mixing and tidal mixing are worthy to be explored in the BS.

Typhoon, as an extreme weather event, may cause strong responses in the upper ocean, for example, forcing intense waves with $H_s$ up to 15 m and reducing the sea surface temperature (SST) in a few degrees (Ginis, 2002). BS locates on the west side of the Pacific Ocean, and is often affected by storm surges and occasionally hit by tropical storms. WB, as an important process in the ocean dynamics, has vital influences on upper ocean turbulence, temperature structure, and boundary layer thickness, etc. Therefore, understanding the role of WB under typhoons (tropical storms) is meaningful to accurately simulate BS dynamic processes, and to improve the disaster forecasting models.

The present WB parameterizations are mainly based on the turbulence closure schemes, many are on the basis of the methods proposed by Mellor and Yamada (1974). Craig and Banner

Foundation item: The Grant from Guangxi Key Laboratory of Marine Environment Change and Disaster in Beibu Gulf under contract No. 2021KF03; the National Natural Science Foundation of China under contract Nos 42176020 and 42076007; the Foundation from Key Laboratory of Marine Environmental Information Technology, Ministry of Natural Resources of China under contract No. 2020GKF-0812; the Tianjin Natural Science Foundation under contract No. 18JCYBJC84900.

*Corresponding author, E-mail: dengzengan@163.com

†These authors contributed equally to this work.

(1994) proposed a WB parameterization method based on the Mellor-Yamada 2.5 (M-Y2.5) turbulence closure scheme. In this method, the wave energy factor $\alpha_{CB}$ is introduced into the boundary condition of the turbulent energy equation to represent the TKE injected by WB. Considering the growth of waves, they found that when $\alpha_{CB}$ is 100 the calculated turbulent dissipation is consistent with the observation. Terray et al. (1999) considered that $\alpha_{CB}$ is a function of waveage, and the typical value is ~150. Besides, Kraus and Turner (1967), Denman and Miyake (1973), Gaspar et al. (1988) also put forward different values of $\alpha_{CB}$ according to their respective researches, and some of them have enormous differences.

Taking account of WB, the sea surface roughness will increase markedly, and the sea surface turbulent microscale will be further influenced. At present, the generally accepted determination method of sea surface roughness is referred to the Charnock relationship in the atmosphere (Donelan, 1990; Smith et al., 1992; Toba et al., 2001; Janssen, 2001), and the Charnock number $\beta$ is introduced into WB parameterization. Indicated by experiments and observations, Bye (1988) suggested that the value of $\beta$ is ~1 400 in the ocean, while Stacey (1999) proposed $\beta$ to be $O(10^5)$ utilizing the Charnock relationship (Charnock. 1955). Mellor and Blumberg (2004) parameterized $\beta$ to $2\times10^5$ in numerical simulations. Gemmrich and Farmer (1999) and Drennan et al. (2005) also suggested different values for $\beta$. Zhang et al. (2011) utilized M-Y2.5 scheme together with WB parameterization to discuss the sensitivity of SST to $\beta$. The study suggested an optimal combination that $\alpha_{CB}$ is about 167 and $\beta$ is about $4.1\times10^5$, based on which the daily and monthly changes in SST were more accurately reflected.

Empirical constants are usually used to estimate $\alpha_{CB}$ and $\beta$ in the present WB parameterization. However, under extremely high wind speeds, empirical $\alpha_{CB}$ and $\beta$ obtained from the simple wind-wave relationship are not applicable (Zhang et al., 2011). Compared with using empirical constants, applying the wave variables from the coupled wave-current model can reflect the influence of wave-induced turbulence more precisely. Therefore, this study adopts the Simulating Waves Nearshore-Princeton Ocean Model (SWAN-POM) one-way coupled model to simulate the dynamic processes under typhoon event (Matsa), and conducts diagnostic experiments to analyze the mechanism of WB in BS during Matsa. Finally, the results of this study are compared with the research on tidal mixing (Deng and Zhao, 2020) to further discuss the characteristics of WB and tidal mixing under typhoon condition, and explore their influences on BS dynamic processes.

## 2 Methods

### 2.1 *Ocean current model*

Princeton Ocean Model (POM) is a baroclinic primitive equation model established by Blumberg and Mellor (1987). In this study, the three-dimensional POM with the M-Y2.5 turbulence closure scheme is used. The turbulent energy equation in the turbulence closure scheme of Mellor (2001) (M01),

$$\frac{\mathrm{D}q^2}{\mathrm{D}t}=\frac{\partial}{\partial z}\left(K_q\frac{\partial q^2}{\partial z}\right)+2K_M\left[\left(\frac{\partial U}{\partial z}\right)^2+\left(\frac{\partial V}{\partial z}\right)^2\right]+\frac{2g}{\rho_0}K_H\frac{\partial\rho}{\partial z}-2\varepsilon+F_q \tag{1}$$

is replaced by turbulent energy equation from Mellor and Blumberg (2004):

$$\frac{\partial q^2}{\partial t}=\frac{\partial}{\partial z}\left(K_q\frac{\partial q^2}{\partial z}\right)+2K_MS^2-2K_HN^2-2\frac{q^3}{B_1l}, \tag{2}$$

where $q^2/2$ is the TKE; $K_M$ is the vertical viscosity coefficient and $K_H$, $K_q$ are the vertical diffusion coefficients; $(U, V)$ are the current velocity components in the directions of $(x, y)$; $\rho$ is the density of seawater and $\rho_0$ is the mean density of seawater; $g$ is the acceleration of gravity; $\varepsilon$ indicates the dissipation and $F_q$ is the horizontal diffusion term of turbulent kinetic energy; $z$ is the vertical coordinate; $t$ is the time; the average velocity shear and the potential density gradient are contained in $S^2$ and $N^2$ respectively, $S^2\equiv\left(\frac{\partial U}{\partial z}\right)^2+\left(\frac{\partial V}{\partial z}\right)^2$; $N^2\equiv-\frac{g}{\rho_0}\frac{\partial\widetilde{\rho}}{\partial z}$; $B_1=16.6$ is a constant; $l$ is the turbulent macroscale.

The vertical mixing coefficient of momentum, temperature and turbulence follow the scheme of Mellor and Yamada (1974, 1982),

$$(K_M, K_H, K_q)=lq\,(S_M, S_H, S_q)\,, \tag{3}$$

where $S_M$ and $S_H$ are functions of $(lN/q)^2$; generally, $S_q$=0.41$S_H$; $(S_M, S_H, S_q)$= (0.30, 0.49, 0.20) near the surface.

The study area covers BS (37.083°–41.033°N, 117.520°–122.470°E), including the Liaodong Bay, the Laizhou Bay, the Bohai Bay, the central sea area, and the Bohai Strait (Fig. 1b). The horizontal resolution is 0.05°×0.05°, and the modeling domain is divided into 80×100 orthogonal rectangular grids. The initial fields, including temperature, salinity, water level, and current, are from the reanalysis dataset of Simple Ocean Data Assimilation (SODA, https://climatedataguide.ucar.edu/climate-data/soda-simple-ocean-data-assimilation). The wind forcing from ERA-interim dataset of the European Centre for Medium-Range Weather Forecasts (ECMWF, https://www.ecmwf.int/en/forecasts/dataset/ecmwf- reanalysis-interim) with resolution of 0.125°×0.125° and interval of 6 h, and the heat flux data from the National Center for Environmental Prediction (NCEP, https://psl.noaa.gov/data/gridded/data.ncep.reanalysis2.html) with an interval of 6 h are adopted and interpolated to model grids. The wind field of typhoon Matsa is also from the ERA-interim of ECMWF, with a resolution of 0.125°×0.125° and an interval of 6 h. The bathymetry is derived from the ETOPO2 dataset of the National Oceanic and Atmospheric Administration (NOAA, https://www.ngdc.noaa. gov/mgg/global/etopo2.html). Twenty-one $\sigma$-levels are specified in the vertical and all the outputs are interpolated to the 21 $Z$-layers (0 m, 1.25 m, 2.5 m, 3.75 m, 5 m, 7.5 m, 10 m, 12.5 m, 15 m, 17.5 m, 20 m, 22.5 m, 25 m, 27.5 m, 30 m, 32.5 m, 35 m, 42.5 m, 50 m, 57.5 m, 65 m). The time step of POM is 200 s in internal mode, and 0.33 s in external mode.

The integration time of the spin-up run is a year, from July 1, 2004 to July 31, 2005. The diagnostic experiments started on August 1, 2005. Four main tidal components (semi-diurnal tide $M_2$ and $S_2$, and diurnal tide $K_1$, $O_1$) are added as the boundary conditions at the model opening boundary. The tidal harmonic constants are provided by the three-dimensional barotropic tide model of the Bohai Sea and the East China Sea (Han et al., 2006). The baroclinic water level at the opening boundary is obtained from the reanalysis dataset of SODA (https://climatedataguide.ucar.edu/climate-data/soda-simple-ocean-data-assimilation).

### 2.2 *Ocean wave model*

The Simulating WAves Nearshore (SWAN) is a third-generation wave model, which can predict sea surface gravity waves

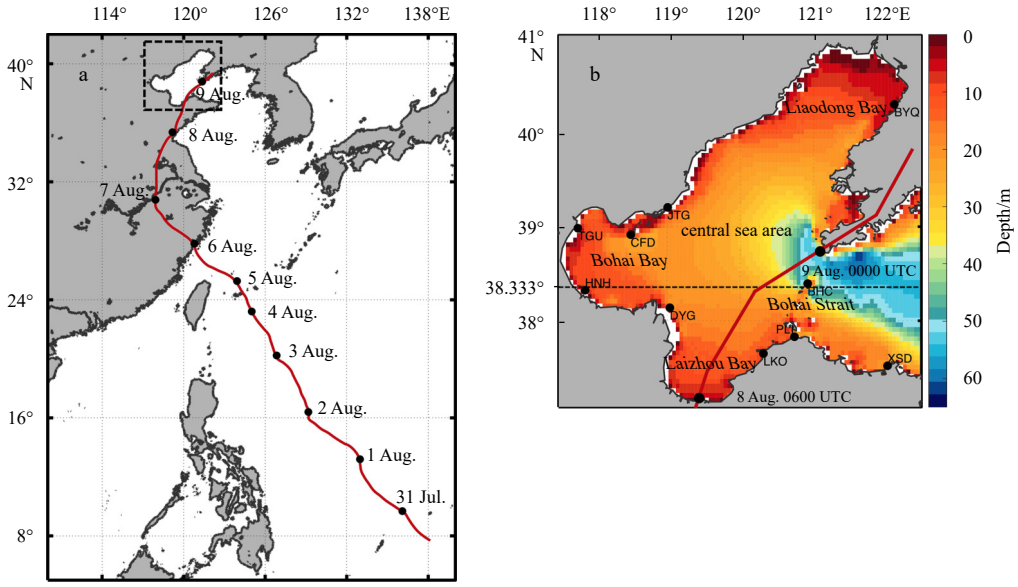


**Fig. 1.** Path of typhoon Matsa (a); topography of the Bohai Sea (BS) and locations of selected tide gauge stations in the BS (b).

well in coastal areas such as estuaries, lakes, and coasts (Booij et al., 1999; Zhao and Sun, 2013). In this study, a two-dimensional non-constant mode is used in the SWAN model, and the physical processes include shallow water breaking, bottom friction, wave-wave interaction, and wave refraction. The horizontal resolution of SWAN is 0.05°×0.05°, coherent with POM. The wind forcing is the same as POM. The spectral action volume is discretized into 32 logarithmically spaced frequencies, with the smallest frequency of 0.05 Hz, and the spectral action volume direction is equally divided into 36 directions with an interval of 10°. The JONSWAP spectrum is specified as the initial and the boundary conditions. The time step of the SWAN model is 200 s, which is consistent with the internal mode time step of POM, and the time interval of the output wave spectrum is 6 h, which is the same as the input time interval of the driving field of POM.

### 2.3 *Wave breaking parameterization*

In general turbulent closure scheme (Mellor and Durbin, 1975), the boundary conditions of the turbulent energy equation on the atmosphere-ocean interface are the same as those on the atmosphere-solid interface (Mellor and Yamada, 1982), such as

$$q^2 = B_1^{2/3} u_*^2, \tag{4}$$

where $u_*$ is the friction velocity.

However, the motion and breaking of sea surface wave make more complicated physical processes in the upper ocean, so that the boundary condition (4) cannot resolve the influences of these physical processes on the turbulence structure in the mixed layer. For this reason, Eq. (5) considering the impact of WB is utilized as the boundary condition of the turbulent energy Eq. (2) (Mellor and Blumberg, 2004),

$$K_q \frac{\partial q^2}{\partial z} = 2\alpha_{CB} u_{*w}^3, \quad z = 0, \tag{5}$$

where $u_{*w}$ is the water-side friction velocity, $\alpha_{CB}$ is determined according to the empirical formula (Terray et al., 1996; 1997),

$$\alpha_{CB} = 15(C_p/u_{*a})\exp[-(0.04C_p/u_{*a})]^4, \tag{6}$$

where $u_{*a}$ is the air-side friction velocity; $C_p/u_{*a}$ is the wave age; $C_p$ is the phase speed of waves at dominant frequent, calculated from the wavelength and the peak wave period.

$u_{*w}$ and $u_{*a}$ are transformed by Mellor and Blumberg (2004):

$$u_{*a}^2 = (\rho_w/\rho_a)\, u_{*w}^2, \tag{7}$$

where $\rho_w$ and $\rho_a$ are the density of seawater and air, respectively; here takes $\rho_a/\rho_w = 1/900$ (Mellor and Blumberg, 2004).

$u_{*a}$ is related to wind speed and roughness (Terray et al., 1996),

$$u_{*a} = kU_{10}/\ln(10/z_0), \tag{8}$$

where $U_{10}$ is the wind speed at 10 m; $z_0$ is the air-side roughness, which is determined based on the empirical regression relationship of the meteorological observation data at the WAVES stations (Donelan, 1990),

$$z_0/H_s = 1.38 \times 10^{-4}(U_{10}/C_p)^{2.66}. \tag{9}$$

By including WB, the turbulent macroscale $l$ near the sea surface adopts (Terray et al., 1999; Mellor and Blumberg, 2004)

$$l = \max(\kappa z_w, l_z), \tag{10}$$

where $\kappa$ is the von Karman Constant (0.41); $H_s$ is the significant wave height; $z_w$ is the water-side roughness following (Donelan, 1990; Smith et al., 1992; Toba et al., 2001; Janssen, 2001)

$$z_w = \beta u_{*w}^2/g, \tag{11}$$

where $\beta$ is Charnock number, and $g$=9.8 m/s$^2$; Mellor and Blumberg (2004) summarized the works of Donelan (1990), Smith et al. (1992), Janssen (2001), and suggested

$$\beta \cong 665(C_p/u_{*a})^{1.5}. \quad (12)$$

In summary, this study introduces the source term of TKE generated by WB to the upper boundary condition and includes sea surface water-side roughness in the turbulent mixing length equation to determine the WB effect.

### 2.4 *One-way current-wave coupled model*

POM and SWAN are one-way coupled in this study. The specific process is shown in Fig. 2. SWAN simulates the wave variables in BS, and then the output wave parameters from SWAN are used to calculate $\alpha_{CB}$ and $\beta$ required by WB parameterization in POM. It is noted that in order to clearly detect the role of WB in a typhoon case, the feedback effects from currents to waves are not discussed in this work.

### 2.5 *Typhoon Matsa*

We choose Matsa (the 9th typhoon in 2005) to perform a typhoon case study. Matsa was formed at about 900 km east of the Philippines at 1200 UTC on 31 July (Fig. 1a) (Song, 2012; Shao et al., 2015), and stepped into the BS at 0600 UTC on 8 August, with the maximum wind speed of ~20 m/s in the BS. The typhoon eye moved northeast to the central sea area (Figs 3b, c) on the 8th, and the intensity of Matsa was weakened rapidly on the 9th with the maximum wind speed of ~12 m/s (Gao et al., 2009; Liu et al., 2010).

Matsa mainly affected the BS on 8 August and 9 August. We select 7–10 August (4 days) to represent three different stages of the typhoon action. Specifically, 7 August represents the normal weather in summer (pre-typhoon stage), 8 August and 9 August represent extremely weather (during-typhoon stage), and 10 August represents the weather with the disappearing typhoon (after-typhoon stage).

## 3 Model verification

To ensure the reliability of our simulations, some verifications are carried out. Tide harmonic analysis is performed with the observed from the tide gauge stations (Fig. 1b) and simulated water levels at 10 tide gauge stations (Table 1). The average absolute deviations of amplitudes of $M_2$, $S_2$, $K_1$, $O_1$ between observations and simulations are 6.44 cm, 5.53 cm, 5.29 cm, 5.09 cm, and the average absolute deviations of the phase lag are 8.74°, 7.87°, 8.26° and 8.89°. The simulations fit well with the observa-

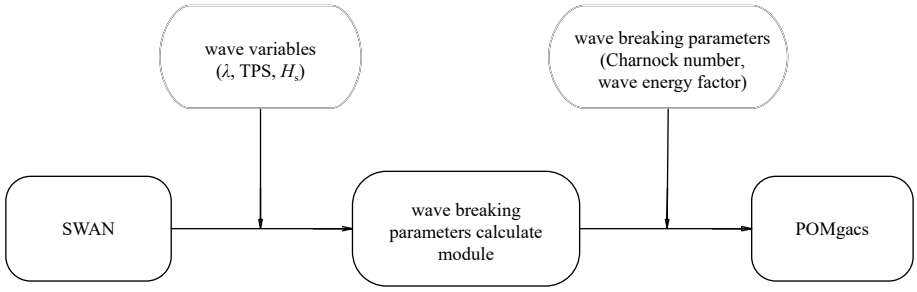


**Fig. 2.** SWAN-POM one-way coupled model.

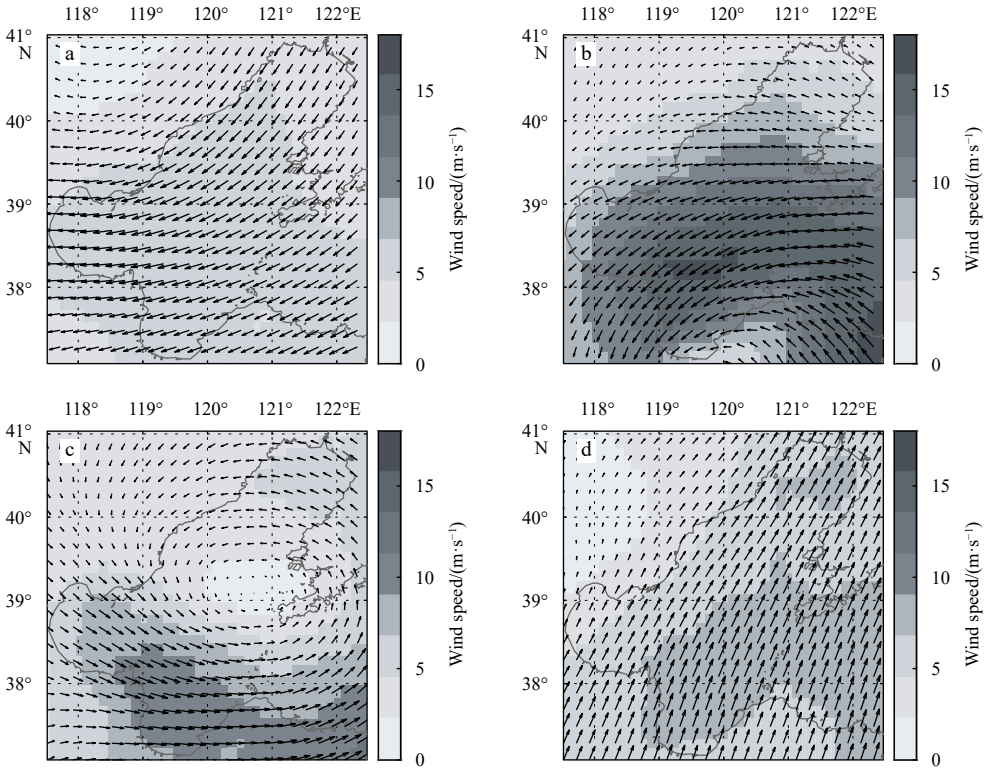


**Fig. 3.** Wind fields at 0000 UTC on 7 (a), 8 (b), 9 (c), and 10 (d) August.

**Table 1.** The absolute deviations of the tidal amplitude and the tidal phase lag between simulations and observations

| Station name | Amplitude /cm | | | | Phase-lag /(°) | | | |
|---|---|---|---|---|---|---|---|---|
| | $M_2$ | $S_2$ | $K_1$ | $O_1$ | $M_2$ | $S_2$ | $K_1$ | $O_1$ |
| BHC | 5.22 | 6.35 | 5.28 | 5.62 | 11.78 | 4.50 | 8.08 | 0.74 |
| BYQ | 8.97 | 9.10 | 2.18 | 6.10 | 8.99 | 10.06 | 7.92 | 12.06 |
| CFD | 5.35 | 4.32 | 7.65 | 2.48 | 3.09 | 8.42 | 7.55 | 8.29 |
| DYG | 4.87 | 7.92 | 1.62 | 0.41 | 3.64 | 13.84 | 9.84 | 8.10 |
| HNH | 2.84 | 2.13 | 10.51 | 4.62 | 7.26 | 9.01 | 6.72 | 9.33 |
| JTG | 6.96 | 9.06 | 9.16 | 7.57 | 1.01 | 9.95 | 10.55 | 11.89 |
| LKO | 7.29 | 4.33 | 4.45 | 4.14 | 15.74 | 2.56 | 8.98 | 7.67 |
| PLI | 7.08 | 5.22 | 3.88 | 7.17 | 7.71 | 4.41 | 8.06 | 10.14 |
| TGU | 10.42 | 3.14 | 0.73 | 8.85 | 15.60 | 8.22 | 7.20 | 7.63 |
| XSD | 5.43 | 3.75 | 7.42 | 3.90 | 12.60 | 7.69 | 7.67 | 13.07 |
| Average absolute deviation | 6.44 | 5.53 | 5.29 | 5.09 | 8.74 | 7.87 | 8.26 | 8.89 |

tions (Fig. 4), and the scatters are distributed on both sides of the line ($y$=$x$) randomly, proving the simulations are reliable.

To further testify the simulations, the simulated SSTs are compared with the observations from the Aqua satellite (from NASA OceanColor Web, https://oceancolor.gsfc.nasa.gov) (Fig. 5b). It is manifested that the simulated monthly-mean SSTs are consistent with the observations, especially in the Bohai Bay, the Laizhou Bay, the Liaodong Bay, the Bohai Strait, and some deviations exist in the western and northern central sea area. The mean absolute deviation of SST is 0.83°C in BS.

Wave parameters are very important to WB parameterization, so it is necessary to validate them. Here the simulated $H_s$, peak wave period (TPS) and wave direction (WD) are compared to the ERA-interim reanalysis product from ECMWF (0.125°×0.125°). At the pre-typhoon stage, the deviations are tiny (Figs 5c, d), and there are small increases during the typhoon action. Although the simulations have certain deviations, especially during the typhoon period, there is no obvious systematic error. The average absolute deviations of hourly-mean $H_s$, TPS and WD (from 7 to 10 August) are 0.086 m, 0.10 s and 9.81°, respectively. The corrsponding correlation coefficients are 0.952 2, 0.983 5, and 0.970 4. The above verifications all prove that the simulated results from our model can generally reflect the dynamic processes in BS, and are basically accurate and reliable.

## 4 Results

Both diagnostic experiment WAVE-WB (with WB) and coordinate experiment WAVE-NON (without WB) are conducted in this study. Hourly model outputs from 7 to 10 August are used to analyze the influences of WB on dynamics and processes (wave variables, mixing coefficient, temperature, mixed layer depth, and current). The 38.333°N section crosses the central sea area and the center of the Bohai Strait, which is the widest section in BS. Therefore, profiles of various parameters along 38.333°N are investigated in detail. The deviations that represent the WB effects are generated by (WAVE-WB)–(WAVE-NON).

### 4.1 *Wave parameters*

According to the statistics of waves from 1950 to 2011 (Ren et al., 2016), the average $H_s$ in BS is 0.7–1.1 m (~0.7 m in 2005) in summer, the smallest in all seasons. $H_s$ simulated by both WAVE-WB (Fig. 6) and WAVE-NON agrees with the value given by Ren et al. (2016). The responses of the $H_s$ to typhoon during 7 and 10 August are basically following the intensity of wind forcing.

$\alpha_{CB}$ is an empirical parameter related to WB-induced TKE, with the magnitude of $O\left(10^2\right)$ (Craig and Banner, 1994; Terray et al., 1996). For mature waves, $\alpha_{CB}$ is ~57, and is ~146 for younger waves (Terray et al., 1996, 1997; Craig and Banner, 1994; Stacey,

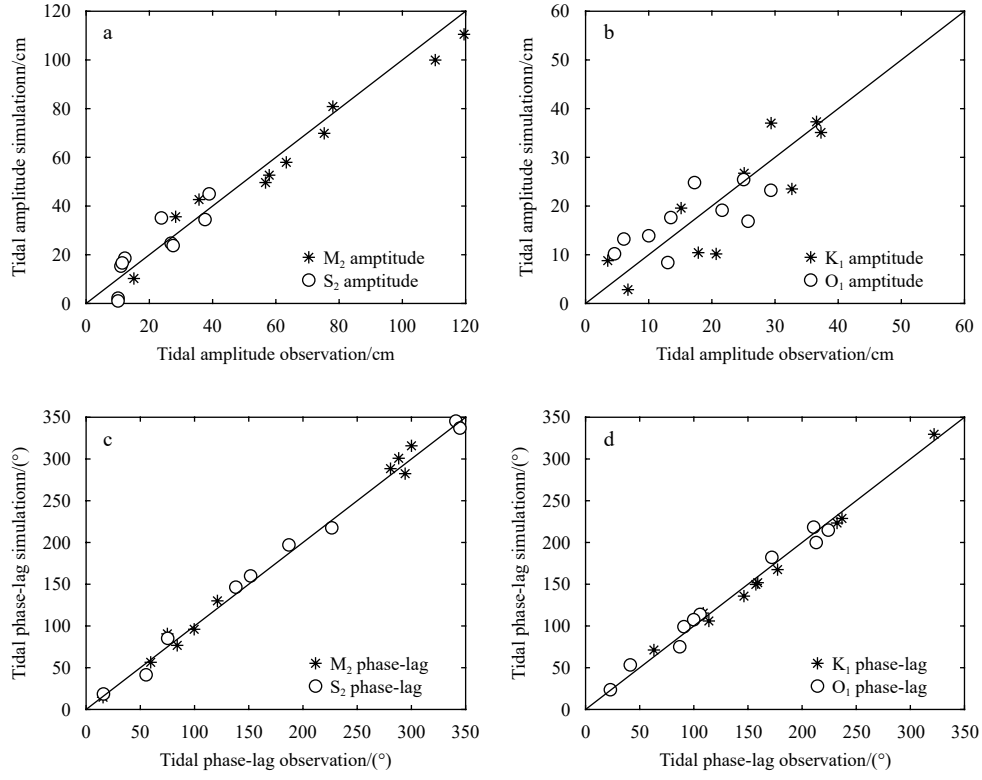


**Fig. 4.** Simulated and observed tidal harmonic constants at tide gauge stations in the Bohai Sea amplitude of $M_2$, $S_2$ (a); amplitude of $K_1$, $O_1$ (b); phase lag of $M_2$, $S_2$ (c); phase lag of $K_1$, $O_1$ (d).

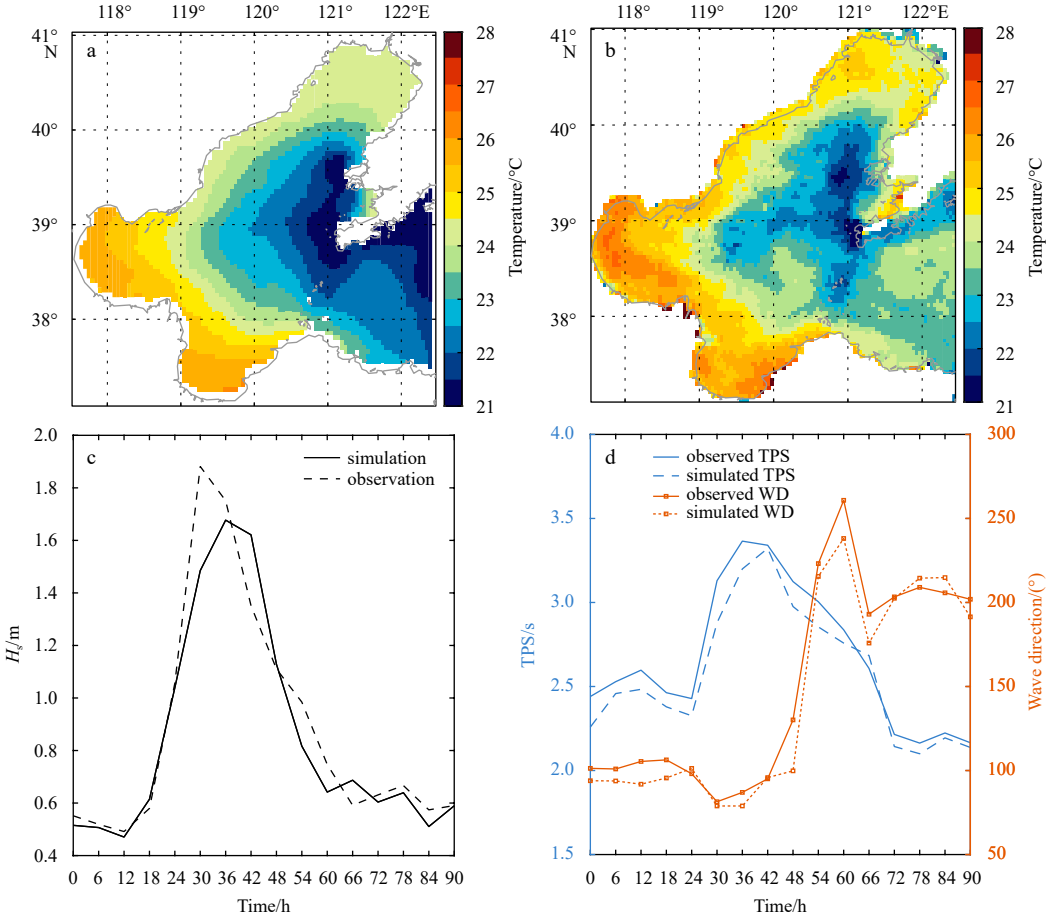


**Fig. 5.** Monthly-mean simulated sea surface temperature (SST) (a); satellite remote sensing SST in August (b); hourly regional-averaged significant wave heigh from simulation and observation (c); hourly regional-averaged peak wave period (TPS) and wave direction (WD) from simulation and observation during 7 and 10 August (d).

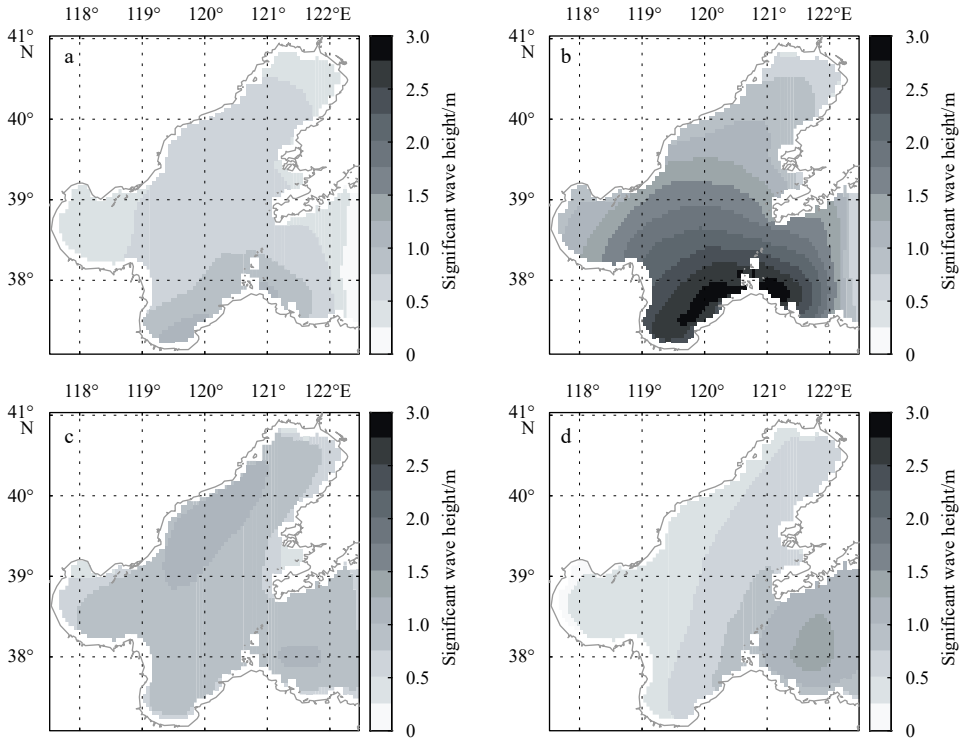


**Fig. 6.** Significant wave height at 0000 UTC on 7 (a), 8 (b), 9 (c), and 10 (d) August.

1999; Mellor and Blumberg, 2004). The wave energy factor is roughly negatively correlated with the wind speed (Figs 7a, d, g, j). On 9 August, the typhoon eye is located between the Bohai Strait and the Liaodong Bay, and $\alpha_{CB}$ near the typhoon eye is larger than that in other regions, suggesting the TKE injected into the surface by winds is more intensively inside the cyclone, while $\alpha_{CB}$ at the center of the cyclone is abnormally small, demonstrating that the vertical mixing in this area is extremely weak. Generally, $\alpha_{CB}$ is linearly associated with the typhoon action, and our estimation is thought to be rational.

$\beta$ is a key parameter for estimating the water-side surface roughness $z_w$, with the magnitude of $O\left(10^5\right)$ (Stacey, 1999; Mellor and Blumberg, 2004). $z_w$ is also roughly negatively correlated with wind speed as shown in Figs 7b, e, h and k. $z_w$ is related to $\beta$, and is of the same magnitude as $H_s$. In this study, $z_w$ is estimated to be in the range of 0.2–1 m (Figs 7c, f, i, l), similar to $H_s$ (Fig. 6). It is indicated that the estimated wave parameters for WB parameterization are reasonable.

Under high wind speed condition, there is a significant increase (Fig. 8) in TPS, which is closely related to WB (Polton et al., 2003). TPS increases as the increasing of wind speed, so that the WB effect depth is deepened. The wind speed reaches the highest value on the 8th but TPS peaks on the 9th, denoting that the response of waves to the typhoon has a lag.

### 4.2 *Mixing*

The vertical viscosity coefficient $K_M$, which is obtained from Eq. (3), is an index to evaluate the vertical mixing strength.

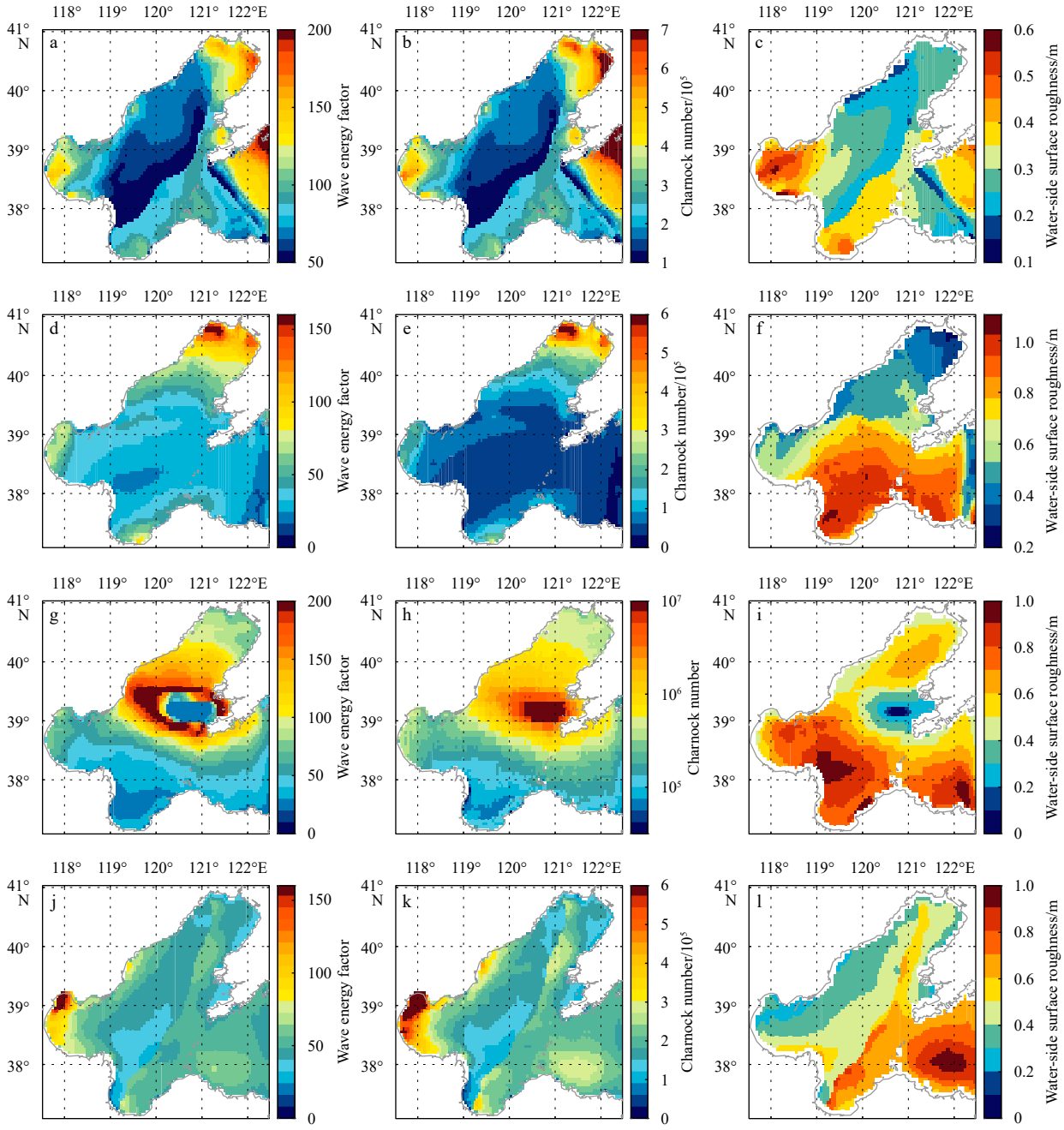


**Fig. 7.** Horizontal distribution of wave energy factor at 0000 UTC on 7 (a), 8 (d), 9 (g), and 10 (j) August; Charnock number at 0000 UTC on 7 (b), 8 (e), 9 (h), and 10 (k) August; water-side surface roughness at 0000 UTC on 7 (c), 8 (f), 9 (i), and 10 (l) August.

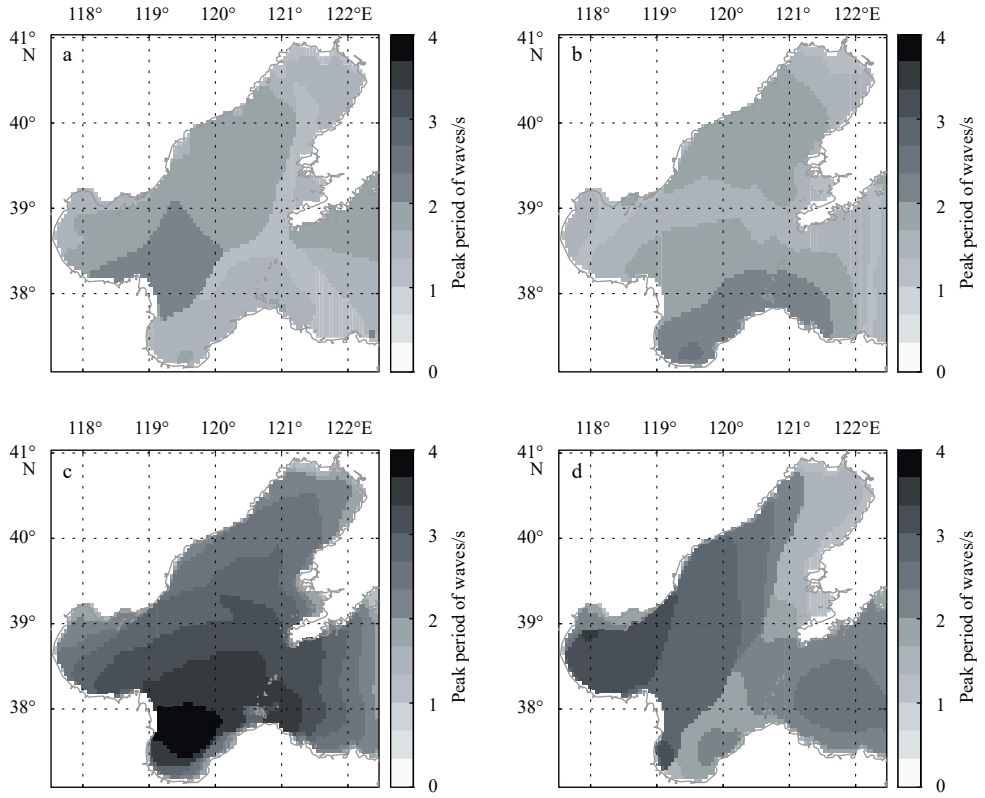


**Fig. 8.** The peak period of waves at 0000 UTC on 7 (a), 8 (b), 9 (c), and 10 (d) August.

Without WB, $K_M$ at the sea surface (Figs 9a, c, e, g) is basically positively related to wind speed, since wind can directly affect the vertical mixing. Including WB, $K_M$ is further modulated, consequently resulting in an integral increase of turbulent mixing in BS (Figs 9b, d, f, h).

Under normal weather, the WB-induced $K_M$ change is relatively small, ranging from ~0.001 m²/s to ~0.01 m²/s (Fig. 9b). High wind speeds have a visible effect on aggravating the turbulence mixing generated by WB. At the during-typhoon stage, the surface $K_M$ change rapidly raises to a level of 0.01–0.15 m²/s, approximately 10 times of that at pre-typhoon stage (Fig. 9d). When wind speed is reduced to below 10 m/s, the WB-induced mixing is decreased to an order of 0.01 m²/s (Fig. 9f), and an abnormally small $K_M$ (close to 0 m²/s) appears at the typhoon eye, implying that the vertical mixing in the vicinity of typhoon center is particularly slight. The relatively large $K_M$ is concentrated in the areas with high wind speeds (the Laizhou Bay and the southern Bohai Strait). It is indicated that the influence of WB on the turbulent mixing is highly dependent on the wind speeds. Although the wind speeds in most area of BS are less than 8 m/s at after-typhoon stage (Fig. 3d), WB still notably affects $K_M$, but the trend is toward the normal weather state. At all the three stages, WB significantly enhances the vertical mixing in the region east of 120°E along 38.333°N (Fig. 10).

In addition, the differences in $K_M$ between WAVE-WB and WAVE-NON decrease with the increasing depth (Figs 10c, f, i, l). Forced by Matsa winds, the surface wind energy injection is enhanced, deepening the impact depth of WB from ~5 m to ~10 m. Overall, WB strengthens the turbulent mixing intensity on the upper ocean, and this action responds rapidly to typhoon forcing.

### 4.3 *Temperature*

The SSTs simulated by WAVE-WB are smaller than the that by WAVE-NON (Fig. 11). Before the typhoon, the SST cooling induced by WB is relatively slight (~0.4°C), and the impact depth is limited to the range above 20–30 m isobath (Fig. 11a). When the typhoon stepping into the BS, WB is intensified by the increasing winds as well as the deteriorating sea conditions, and the seawater "cold absorption" phenomenon is further enhanced, therefore SST drops rapidly (with maximum of ~1°C) (Fig. 11b). On 9 August, WB causes a wider cooling (Fig. 11c) in the BS. The SST differences in the entire central sea area and the Bohai Strait are added (the maximum exceeds 1.2°C). This phenomenon demonstrates that the continuous effect of WB brings deeper and colder water up to the surface. Although the intensity of typhoon on 9 August is weakened and the $K_M$ reaches its maximum on the 8th, the response of SST gets its maximum on the 9th, evidencing that there is a hysteresis in temperature changes. After the typhoon, the SST differences are still greater than that at pre-typhoon stage. This continuous cooling reveals that WB, under the action of typhoon, not only affects the SST but also impacts the total heat budget in the BS.

In the vertical, a stably vertical temperature stratification exists in the normal weather of summer (Fig. 12a), and WB usually makes SST slightly lower (~0.3°C) and increase the water temperature within ~10 m depth below the sea surface (Fig. 12b). At the beginning of typhoon, since the duration of the typhoon forcing is still short, the vertical temperature structure does not change drastically. The surface layer temperature change is greatest (up to ~1°C) in the region of 120°–122.5°E, and the impact depth is ~15 m (Fig. 12f). One day after the acting of Matsa, the upper seawater is mixed sufficiently, breaking the stratification within 5 m depth, and the impact penetrates deep to ~20 m (Fig. 12j). If the typhoon could last longer, WB would cause a more intensively heat exchange. After the typhoon, the temperature variation

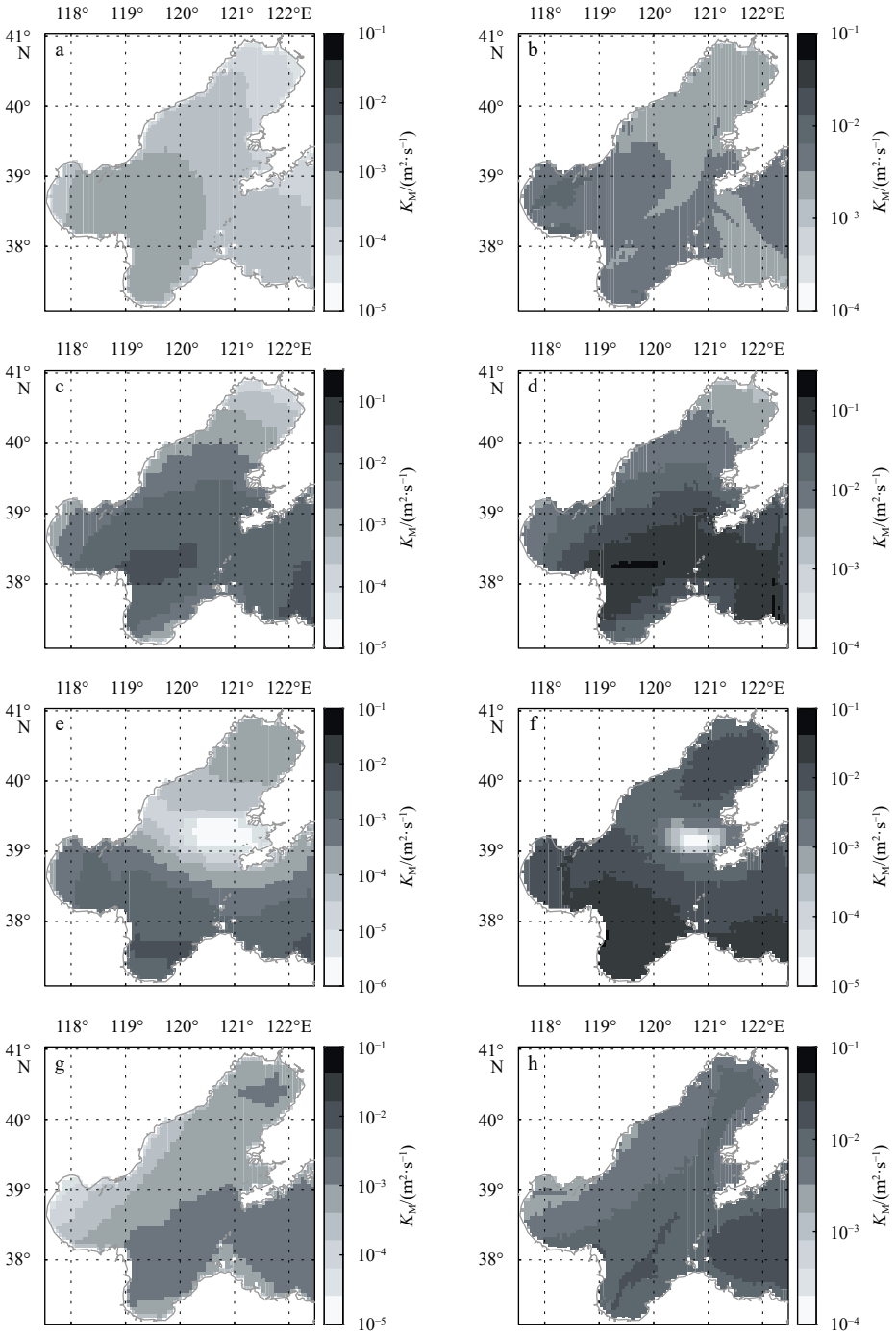


**Fig. 9.** Surface $K_M$ simulated by WAVE-NON at 0000 UTC on 7 (a), 8 (c), 9 (e), and 10 (g) August; $K_M$ differences ((WAVE-WB)–(WAVE-NON)) at 0000 UTC on 7 (b), 8 (d), 9 (f), and 10 (h) August.

caused by WB remains significant, which again reflects the hysteretic effect of temperature in response to the typhoon.

### 4.4 *Mixed layer depth*

Yablonsky and Ginis (2008) defined mixed layer depth (MLD) as the depth of the water layer at a temperature difference of 0.5°C from the sea surface. Here we calculate the MLD in BS following this definition. In normal summer weather, the vertical temperature stratification in BS is obvious. The temperature differences between the surface and subsurface layers are notable, MLD is about 1–2 m. However, the relatively shallow areas near the shore are sufficiently mixed. As water depth increasing, the MLD in the region east of 119°E along 38.333°N rapidly decreases to about 1 m (Fig. 13a), and is slightly deepened (with a increase of ~0.2 m, but there is an obvious increase of ~1.8 m in 120°–121°E) after adding WB.

By the forcing of Matsa, WB renders a significant deepening effect (~2.4 m) on MLD in the relatively deep water zone especially in 120°–121°E (Fig. 13b). On 9 August, the MLD in east of 121°E region simulated by WAVE-NON is greater than 2 m (Fig. 13c), which denotes that the typhoon can directly deepen the MLD. After adding WB, the MLD rapidly deepens to around

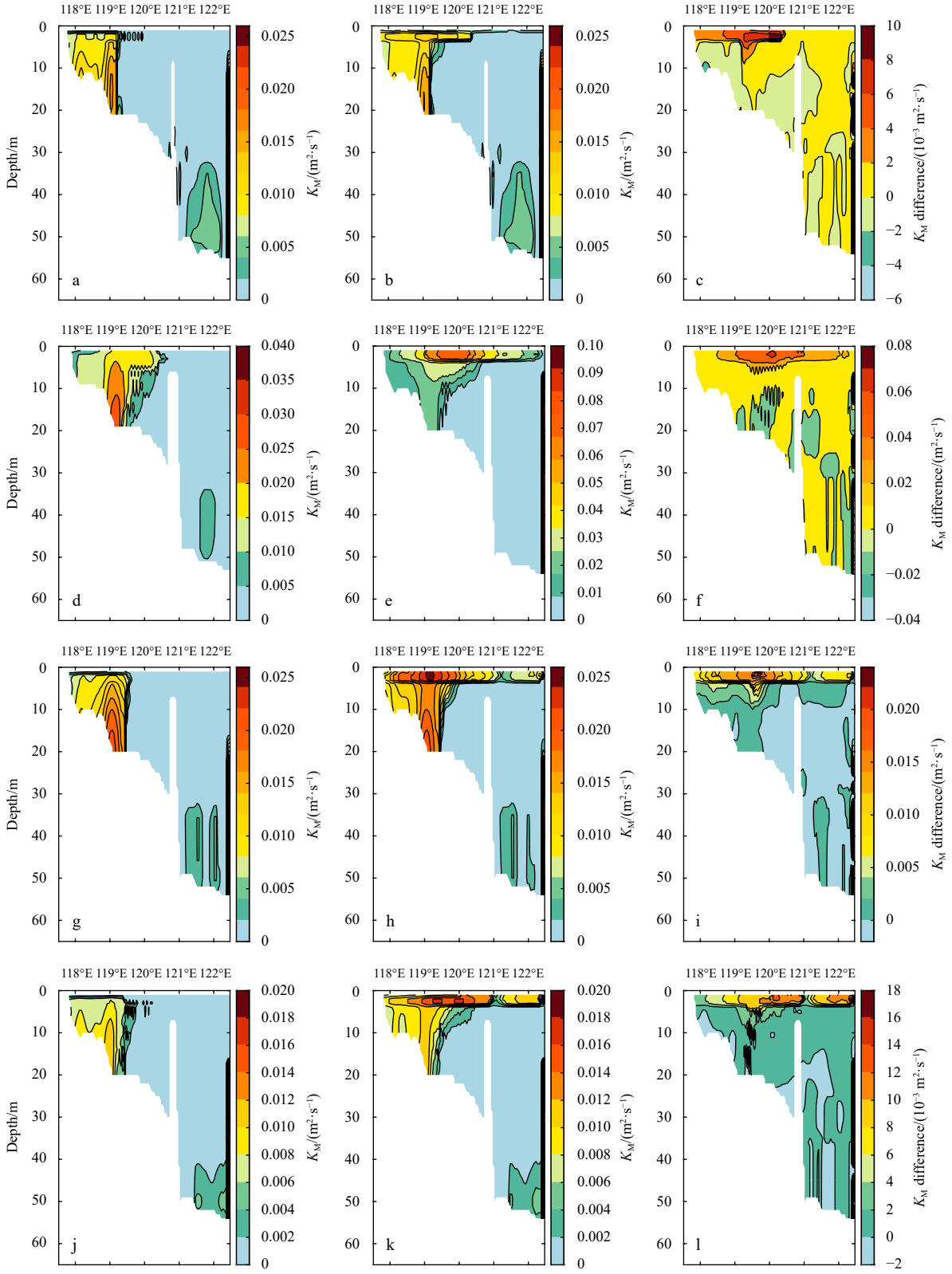


**Fig. 10.** Vertical distribution of $K_M$ along 38.333°N simulated by WAVE-NON at 0000 UTC on 7 (a), 8 (d), 9 (g), and 10 (j) August; by WAVE-WB at 0000 UTC on 7 (b), 8 (e), 9 (h), and 10 (k) August; $K_M$ differences at 0000 UTC on 7 (c), 8 (f), 9 (i), and 10 (l) August.

4.5–7.8 m, signaling that the impact depth of WB is about 1.6–3.6 m. Compared with that at the pre-typhoon stage, typhoon markedly intensifies the impact of WB on MLD. Contrasting with the temperature profile, we infer that the water above MLD is sufficiently mixed. When the typhoon is disappeared, the WB impact retreats to the depth of about 0.8–3.5 m, slightly smaller than that at the during-typhoon stage (Fig. 13d).

From the perspective of the horizontal distribution of MLD,

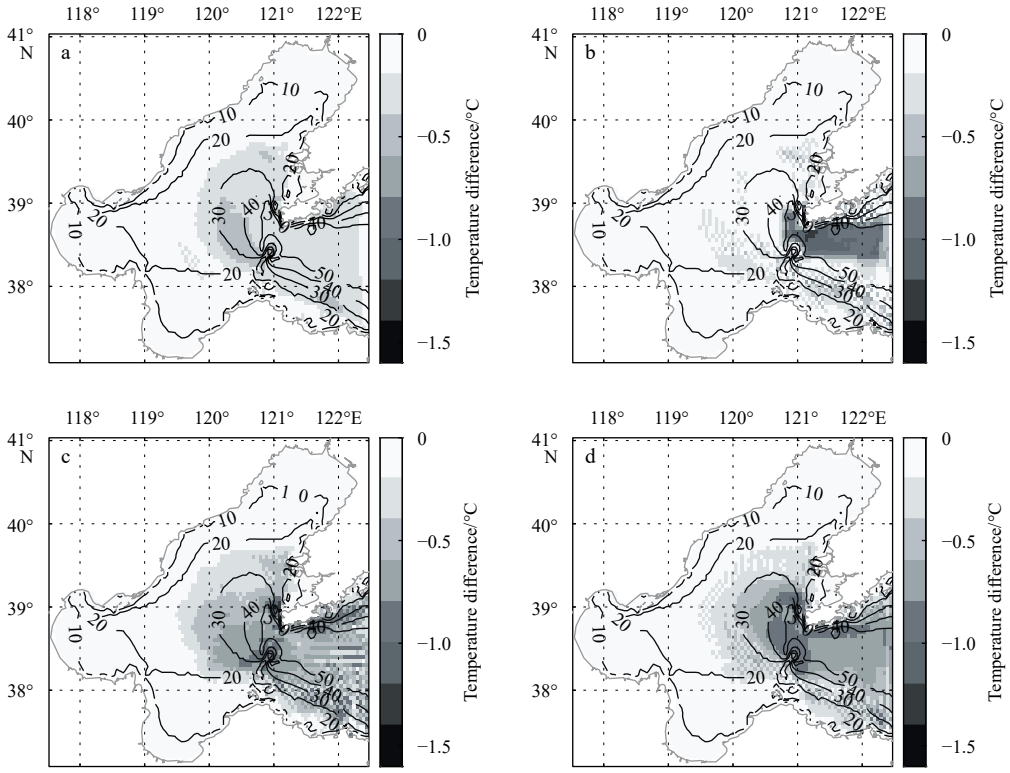


**Fig. 11.** Sea surface temperature differences of (WAVE-WB)–(WAVE-NON) at 0000 UTC on 7 (a), 8 (b), 9 (c), and 10 (d) August. The contours indicate the depth of Bohai Sea.

WB-induced deepening before the typhoon is limited to the central sea area and is relatively weak (Fig. 14b). On the 8th, the impact is expanded to the central sea area, the Bohai Bay and the Liaodong Bay (Fig. 14d). Since the typhoon eye is close to the Liaodong Bay on the 9th, WB has a noticeable impact on MLD in the Liaodong Bay, the central sea, and the northern Bohai Strait, leading to a significant deepening of the MLD (Fig. 14f). After the typhoon, the isoline values become slightly small (Fig. 14h) and the situation is gradually recovering to the state before typhoon.

### 4.5 *Currents*

Before the typhoon, currents in BS generally flow from the Liaodong Bay, the Bohai Bay and the Bohai Strait to the central sea area and the Laizhou Bay. WB does not change the integral direction of currents, but it alters the local flow patterns (Fig. 15b), particularly in the southern part of Bohai Strait and the central sea area (with a maximum speed change of ~0.07 m/s). In particular in a part of the Bohai Bay and the Bohai Strait, the changes in current vectors (CCVs, obtained by (WAVE-WB)–(WAVE-NON)) are consistent with the wind directions (Fig. 15c).

On the 8th, the current speed in the central sea area is decreased (with maximum change of ~0.2 m/s) by WB. In the most areas of BS, the cosine of the current change and the wind direction is –1 (Fig. 15f), suggesting that the CCVs are opposite to the wind vectors, reflecting an interesting phenomenon that hasn't been proposed before: WB has an inhibitory effect on the typhoon-forced current change.

One day after Matsa entering BS, WB-induced speed change is about ±0.1 m/s near the cyclone and the Bohai Strait, and it approaches 0 m/s at the center of the typhoon. Because of the influence of winds, the current direction in the Laizhou Bay is gradually parallel to the wind direction (Fig. 15g), implying that during typhoon the wind is the more important factor in affecting currents than tide. In addition, the CCVs are opposite to the wind direction at the periphery of typhoon, and follow the wind direction near the typhoon eye (Fig. 15i). This phenomenon shows that, around the center of the cyclone, the surface current is more intensively affected by winds, and the CCVs follow the wind direction. While the surface current differences at the periphery of typhoon are slight; WB has an inhibitory effect on wind action. After the typhoon, the current change in the cyclone area follows the direction of wind, spreading from the cyclone center to the surrounding area, and the distribution of CCVs (Fig. 15l) return to in line with that at the pre-typhoon stage.

It is worth noting that the areas with obviously current changes are concentrated in the central sea area and the Bohai Strait, basically overlapped with the areas of marked temperature changes, which suggests that WB exerts significant effects on the turbulent mixing in these areas (Figs 15b, e, h, k and 11).

At the pre-typhoon stage, the impact depth of WB is relatively shallow (~7 m) (Fig. 12d). After Matsa entering BS, the current velocities within the depth of –10 m are more evenly distributed under the action of WB, the resulting changes in speed are ±0.15 m/s (Fig. 12h). However, due to the short duration of typhoon action at this stage, TKE is still limited to a few meters below the sea surface, thus the stratification of currents can only be formed in the area with relatively deep water (east of 120°E). Consequently, the velocity differences between the surface and bottom layers are enlarged. But the deviations are decreased obviously after the typhoon lasting for a day due to the injected TKE can be fully transmitted to the depth of ~14 m. As the disappearance of typhoon, the current profile changes from the surface downwards, forming a temporary current stratification (Fig. 12p). WB promotes the synergistic changes of currents in BS. Thus, to a certain extent, WB weakens the current stratification.

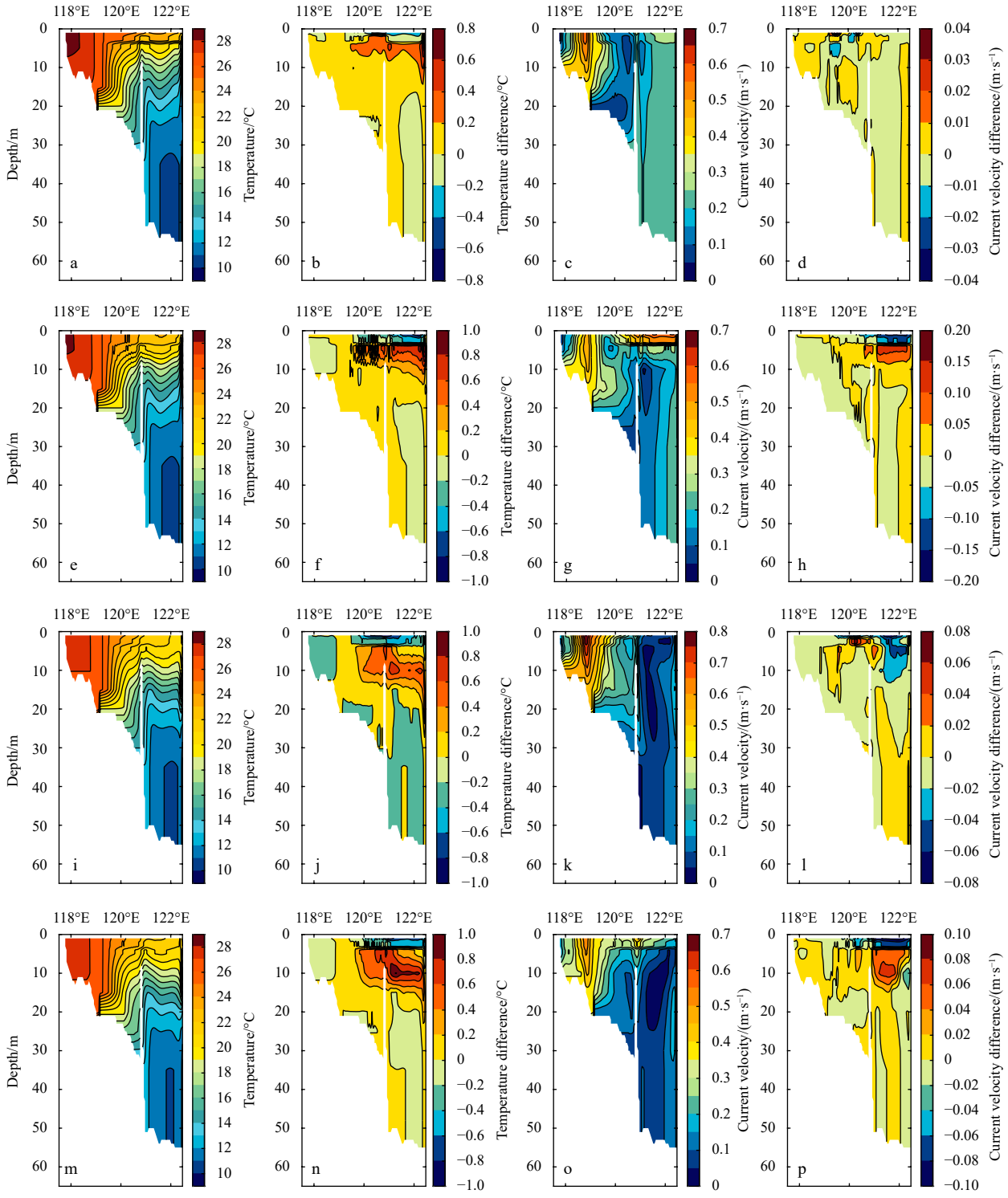


**Fig. 12.** Vertical distribution of temperature along 38.333°N simulated by WAVE-NON at 0000 UTC on 7 (a), 8 (e), 9 (i), and 10 (m) August; temperature differences along 38.333°N at 0000 UTC on 7 (b), 8 (f), 9 (j), and 10 (n) August; vertical distributions of currents along 38.333°N simulated by WAVE-NON at 0000 UTC on 7 (c), 8 (g), 9 (k), and 10 (o) August; current velocity differences along 38.333°N on August at 0000 UTC 7 (d), 8 (h), 9 (l), 10 (p) from 7 August to 10 August.

## 5 Comparisons of WB with tidal mixing

Deng and Zhao (2020) performed a case study of the typhoon Matsa to analyze the impacts of tidal mixing on ocean dynamics in BS. To reveal the different influences between WB and tidal mixing on BS dynamics under typhoon condition, here we conduct a comprehensive comparison (Table 2). From a regional point of view, during Matsa, the tidal mixing coefficient is generally increased in the Bohai Bay, the Laizhou Bay, the Liaodong Bay, and the Bohai Strait, and the effect of typhoon on the tidal mixing in the central sea area is relatively small. Whereas, WB-induced mixing during typhoon increases significantly in the central sea area, the Laizhou Bay, and the Bohai Strait. Both WB-in-

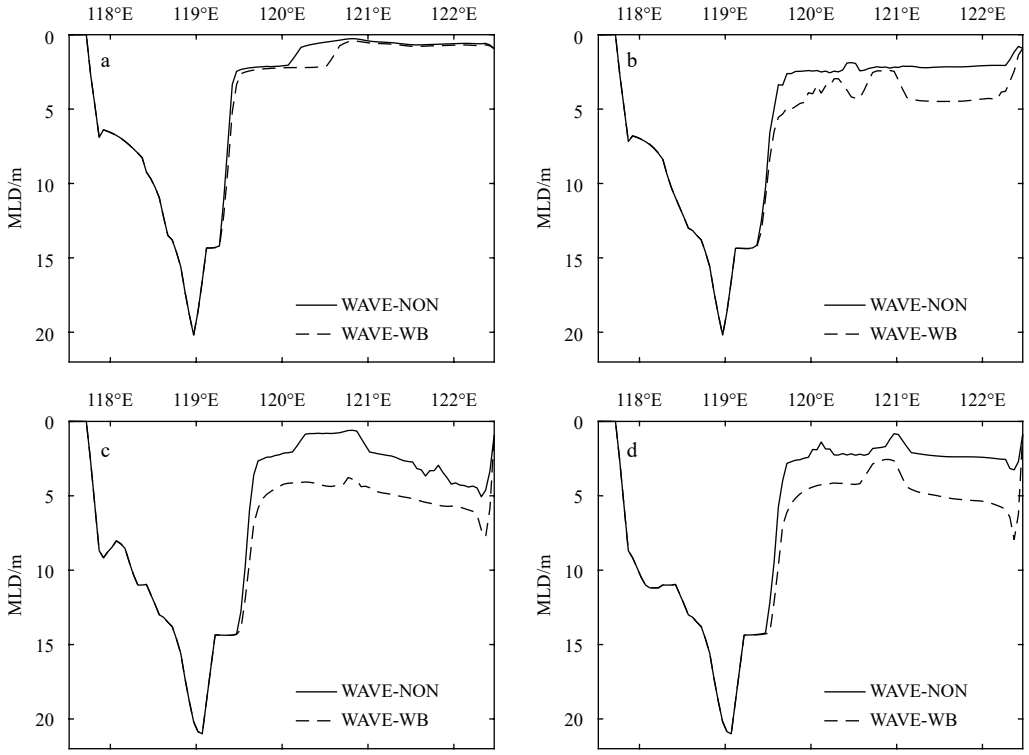


**Fig. 13.** Mixed layer depth (MLD) along 38.333°N simulated by WAVE-NON and WAVE-WB at 0000 UTC on 7 (a), 8 (b), 9 (c), and 10 (d) August.

duced mixing and tidal mixing can be intensified by approximately 1 order of magnitude by typhoon in BS. The mixing caused by WB under typhoon is generally larger than tidal mixing by 1 order, especially in the central sea area, it is about 3 orders (Fig. 9d). During the typhoon, differences between the two mixings are mainly presented in the central sea area. Tidal mixing is greatly affected by the topography, so that in the coastal area (three bay areas) the enhancement is more obviously; while in the offshore deeper water region (the central sea area and the Bohai Strait), the TKE generated by WB makes the mixed layer thicker.

By the continuous forcing of typhoon, the effects of both tidal mixing and WB on temperature are intensified, and the persistent actions of the two effects facilitate the mixing of surface water with deep colder water, resulting in a significant cooling in the central sea area. Although the tidal mixing in the bay areas is very strong, the tidal mixing-related temperature changes are not that noticeable due to the weak vertical stratification and the overall warm water column. The impact of WB on the temperature is the strongest in the central sea area and the Bohai Strait (Fig. 12). In combination of the profile diagram (Fig. 12f) and temperature differences plots at depths of 0 m, 5 m, 15 m, 25 m (Fig. 16), it can be seen that the WB-induced change at 25 m is less than 0.01°C, a trivial effect, demonstrating that at the during-typhoon stage the impact depth of WB (~15 m) is smaller than that of tidal mixing, and the WB's influence on temperature (±1°C) is weaker than that of tidal mixing.

The distribution pattern of currents under typhoon is directly related to wind forcing. Tidal mixing has trivial effect on the structure and magnitude of circulation. However, WB exerts an impact on local current speed and direction, the maximum speed change around the central sea area is about –0.2 m/s. In BS, the cosine values of CCVs and wind directions are almost –1 (Fig. 15), revealing that WB induces an inhibitory effect on the typhoon impact, and this phenomenon can not be found in tidal mixing.

Deng and Zhao (2020) investigated the tidal mixing-resulted water level changes at four stations respectively located in the Bohai Bay, the Laizhou Bay, the Liaodong Bay, and the central sea area near the Liaodong Peninsula, and revealed that tidal mixing would partly compensate for wind forcing and cause alternation in tidal phase. We also investigate the effect of WB on water level under typhoon Matsa, and find that the water level change caused by WB on the 8th is $O(10^{-3})$ (Fig. 17a), and the alternations are within 0.01 m at the four spots from the 8th to 10th (Fig. 17b), which suggests that the impact of WB on the water level is tiny, and there is almost no associated phase change.

## 6 Conclusions

In this study, a one-way coupled wave-current model is used to investigate the influences of WB on ocean dynamics under typhoon weather in the BS. Before the diagnostic experiments, some model verifications (including tidal harmonic constant, SST, $H_s$, TPS, and WD) are carried out, proving that our model is reliable and can generally reproduce the dynamic processes in BS.

The WB-induced turbulent mixing is strongest at the surface layer and gradually weakens as the increasing depth. During the typhoon, $K_M$ is increased apparently, with the largest one of ~0.15 m$^2$/s, reaching ~10 times of that at pre-typhoon stage. Particularly, the WB impact on $K_M$ is close to 0 m$^2$/s at the center of the typhoon. Due to the increase of wind forcing and the deterioration of sea condition, WB brings deeper and colder water up to the surface, consequently increasing the temperature cooling extent (from ~0.4°C to ~1.2°C) and range. In addition, under the continuous acting of the typhoon, WB breaks the vertical stratification at the 5 m water layer, and the impact range deepens from ~10 m to ~20 m.

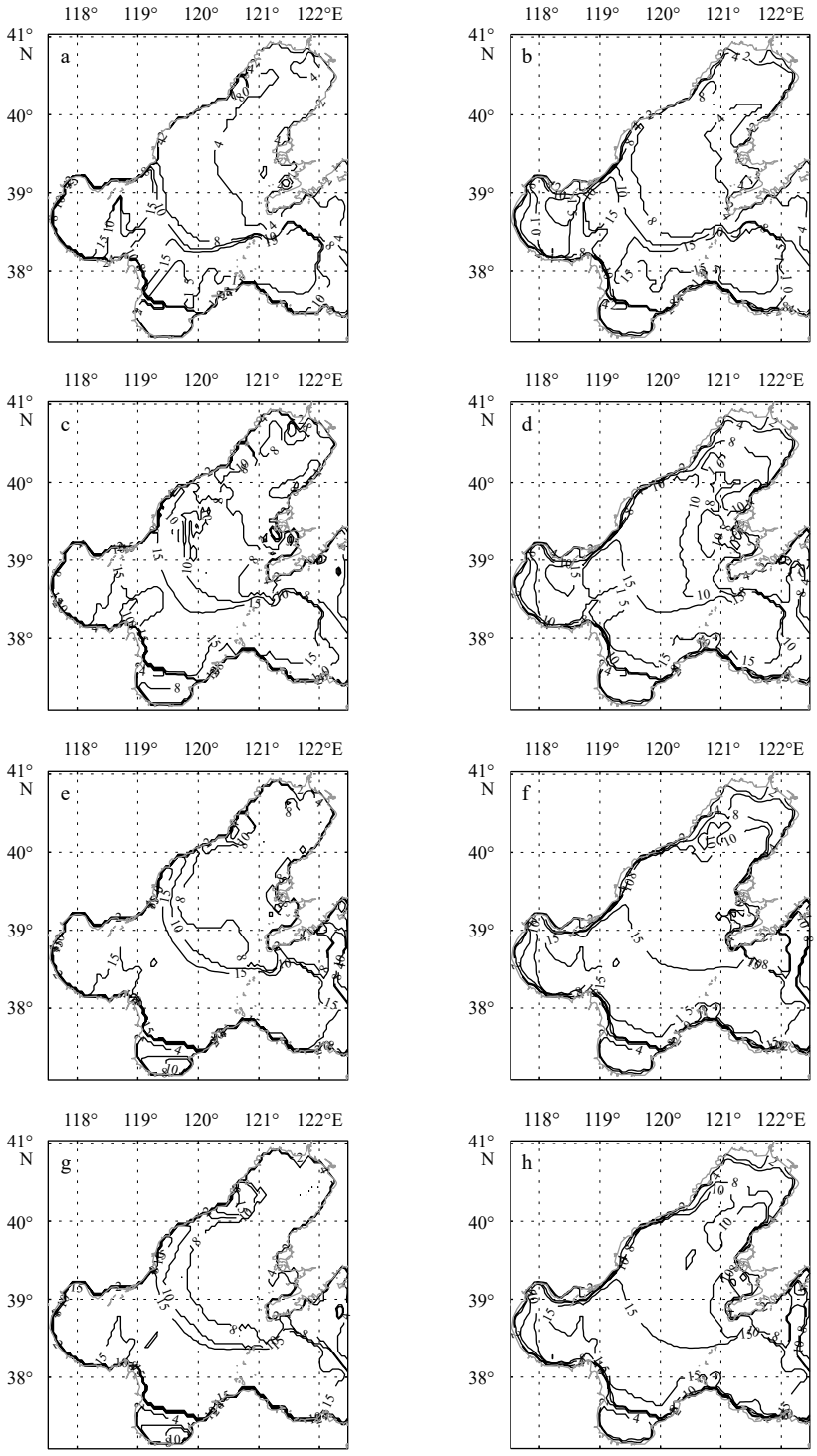


**Fig. 14.** Horizontal distribution of mixed layer depth (MLD) (m) simulated by WAVE-NON at 0000 UTC on 7 (a), 8 (c), 9 (e), and 10 (g) August; by WAVE-WB at 0000 UTC on 7 (b), 8 (d), 9 (f), and 10 (h) August. The contours indicate MLD.

At the during-typhoon stage, WB deepens the mixed layer for about 1.6–3.6 m, and the increase of MLD is largest near the typhoon eye. The influence range also expands from the central sea area to the central sea area, the Liaodong Bay, and the Bohai Strait. WB doesn't change the integral current direction in BS, but it impacts the local flow patterns. Under the action of typhoon, the CCVs caused by WB are almost opposite to the wind direction. The impact depth of WB on current is shallow, with a range of ~7 m in normal weather and ~14 m in typhoon condition.

The areas with maximum change in current basically coincide to the regions with maximum temperature change during the entire typhoon period, inferring that WB has the greatest impact on mixing in those areas. Diagnostic experiments evidence that the influences of WB on temperature are cumulative and have an obviously lag.

Comparing with the research of Deng and Zhao (2020) on tidal mixing, we find that tidal mixing has greater influence on temperature structure, with larger impact range and higher intensity,

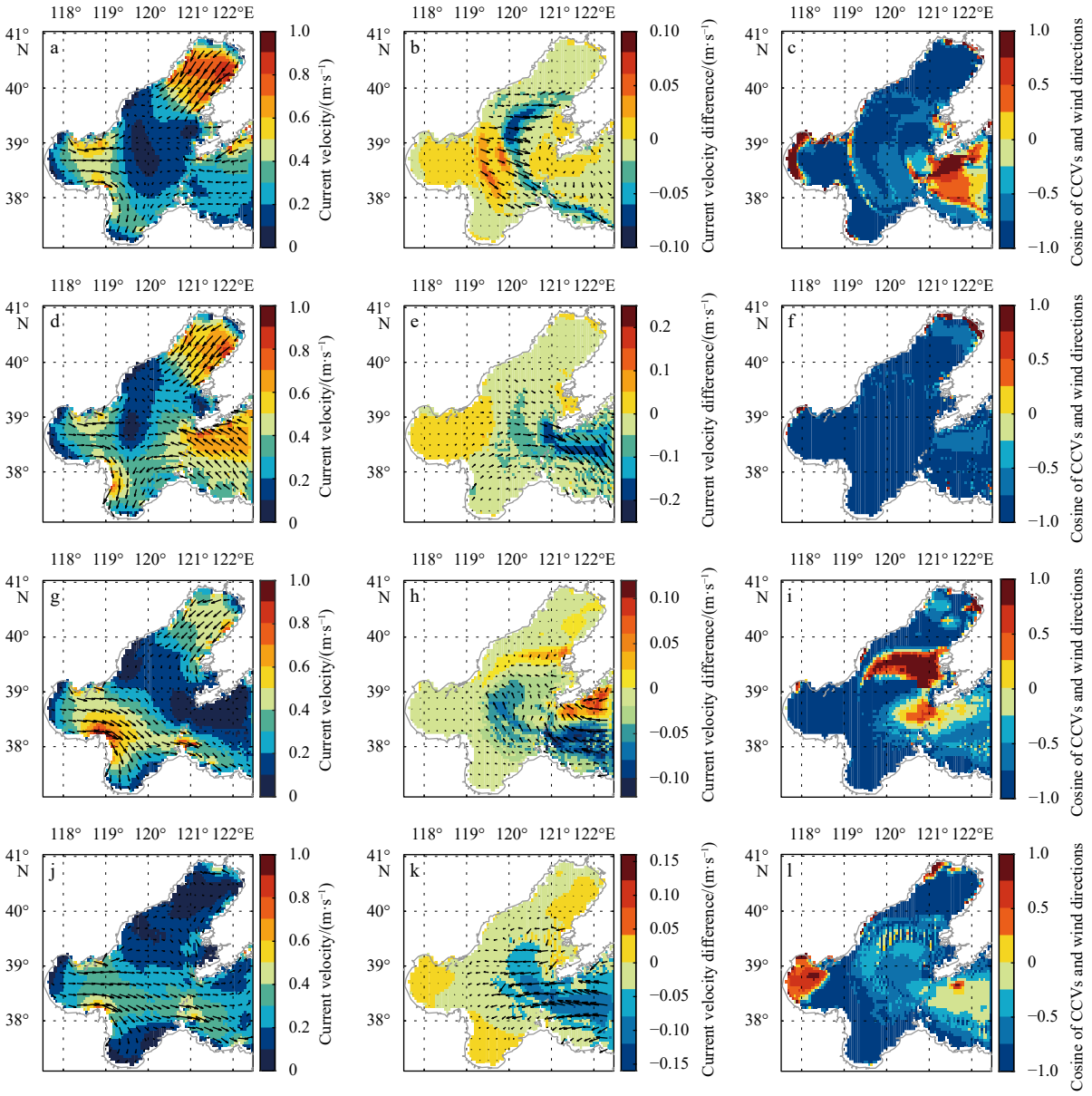


**Fig. 15.** Surface currents simulated by WAVE-NON at 0000 UTC on 7 (a), 8 (d), 9 (g), and 10 (j) August; current difference at 0000 UTC on 7 (b), 8 (e), 9 (h), and 10 (k) August; cosine of CCVs and wind directions at 0000 UTC on 7 (c), 8 (f), 9 (i), and 10 (l) August.

**Table 2.** Comparisons of tidal mixing with wave breaking (WB) in the Bohai Sea (BS) under typhoon

| Variable | Tidal mixing | WB |
|---|---|---|
| Mixing coefficient values | significant on the BS coast:<br>northern Bohai Bay, western Laizhou Bay, eastern and western Liaodong Bay, Bohai Strait: ~$1\times10^{-2}$ m$^2$/s<br>southern Bohai Bay: >$2\times10^{-3}$ m$^2$/s<br>northern Liaodong Bay: >$1\times10^{-3}$ m$^2$/s<br>central sea area: < $1\times10^{-4}$ m$^2$/s | depend on wind:<br>central sea area: ~0.15 m$^2$/s<br>Bohai Strait: 0.06–0.12 m$^2$/s<br>northern Laizhou Bay: ~0.04 m$^2$/s<br>Liaodong Bay, Bohai Bay: <0.01 m$^2$/s |
| Impacts on temperature | impact depth: ~25 m<br>maximum change: ±2.5°C | impact depth: ~15 m<br>maximum change: ±1°C |
| Impacts on current | almost no effect on the current structure | maximum: −0.2 m/s (Bohai Strait)<br>CCVs are almost exactly opposite to the wind direction in BS |
| Impact on water level | cause tidal phase alternation<br>Bohai Bay, Liaodong Bay: −0.04 m<br>Laizhou Bay, central sea area: 0.005–0.033 m<br>Bohai Strait: 0.026–0.068 m | no phase difference<br>−0.01 m<BS<0.01 m |

and it will compensate for wind forcing and cause tidal phase alternation. Whereas, WB has a relatively larger impact on currents and generally inhibits the typhoon forcing. Besides, the tidal mixing effect in the three bay areas of BS is relatively strong,

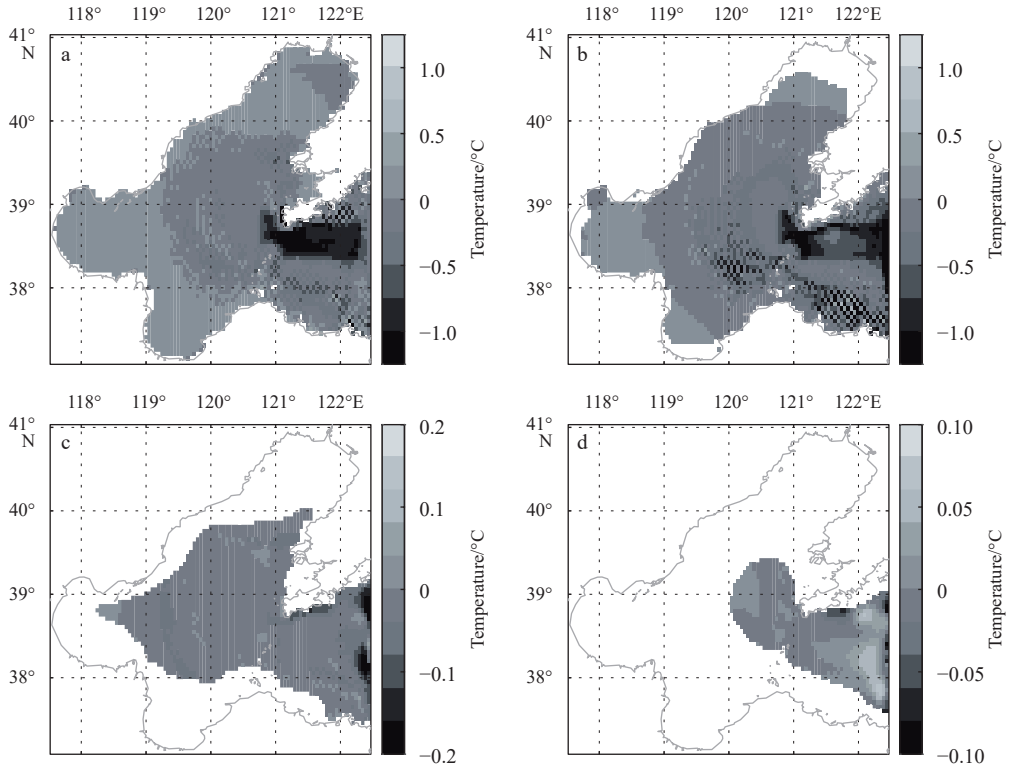


**Fig. 16.** Wave breaking-induced temperature changes at depth of 0 m (a), 5 m (b), 15 m (c), and 25 m at 0000 UTC on 8 August (d).

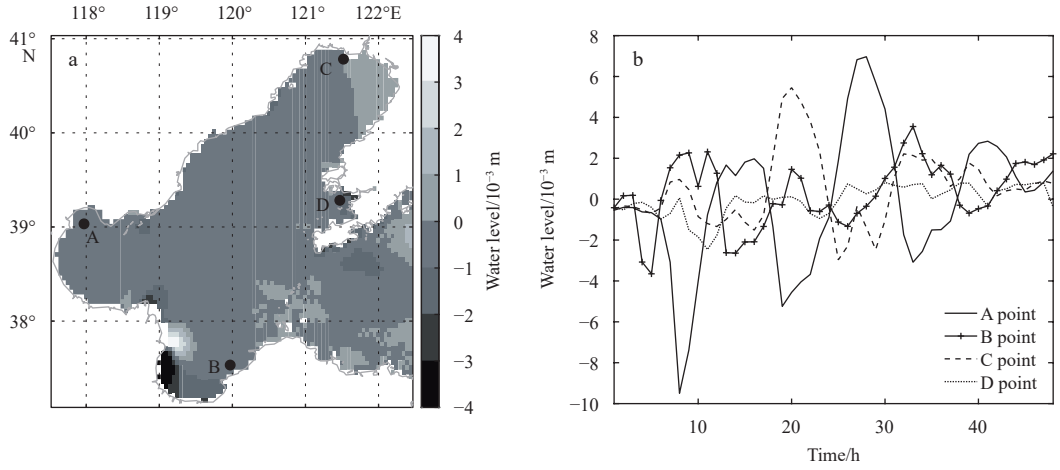


**Fig. 17.** Water level differences caused by wave breaking in the Bohai Sea at 0000 UTC 8 August (a); at locations of A (39.033°N, 117.97°E), B (37.533°N, 119.97°E), C (40.783°N, 121.52°E), D (39.283°N, 121.47°E) from 0000 UTC 8 August to 0000 UTC 10 August (b).

and is generally weak in the central sea area and the Bohai Strait, while the situations of WB are opposite.

This study discusses the effects of WB on dynamics in BS under typhoon conditions. Non-breaking waves such as Langmuir turbulence (LT) also have a significant effect on dynamics. In our previous work, we investigated the effects of LT under common weather (Cao et al., 2019). By a briefly comparison of WB and LT effects, we find that LT can impact the entire mixed layer, while WB only acts within the top several meters. The LT-caused change in $K_M$ increases with depth, reaching a maximum (~0.001 m$^2$/s) in the 35 m layer. The effect of WB on $K_M$ at the sea surface (~0.01 m$^2$/s) is greater than that of LT, but this effect decays rapidly with depth, acting within ~5 m below the sea surface. The temperature change caused by LT in BS is greater than 0.2°C even at the 15 m layer, which is greater than that by WB. The impact of LT on current velocity (~0.1 m/s) is also slightly greater than that of WB (~0.07 m/s). In general, both LT and WB make the vertical current velocity distribution more uniformly.

This research is mainly focused on the impacts of WB on BS dynamics in summer typhoon weather. However, the mechanism and distribution characteristics of WB under common weather in spring and autumn are also worth exploring, which will help us further understand the role of WB in BS. The simulation results of this study still have certain deviations from the realistic ocean state, so that the model would be further improved in the future. Limited by experimental conditions, this study only uses a one-way coupled model. In the future, we will detect the impact of WB using an atmosphere-circulation-wave

fully coupled model, and further conduct a systematic study on the mechanisms of WB, tidal mixing, and LT in BS.

## References


Agrawal Y C, Terray E A, Donelan M A, et al. 1992. Enhanced dissipation of kinetic energy beneath surface waves. Nature, 359(6392): 219–220, doi: 10.1038/359219a0

Blumberg A F, Mellor G L. 1987. A description of a three-dimensional coastal ocean circulation model. In: Heaps N S, ed. Three-Dimensional Coastal Ocean Models. Washington: American Geophysical Union, 1–16, doi: 10.1029/CO004p0001

Booij N, Ris R C, Holthuijsen L H. 1999. A third-generation wave model for coastal regions: 1. Model description and validation. Journal of Geophysical Research, 104(C4): 7649–7666, doi: 10.1029/98JC02622

Bye J A T. 1988. The coupling of wave drift and wind velocity profiles. Journal of Marine Research, 46(3): 457–472, doi: 10.1357/002224088785113559

Cao Yu, Deng Zengan, Wang Chenxu. 2019. Impacts of surface gravity waves on summer ocean dynamics in Bohai Sea. Estuarine, Coastal and Shelf Science, 230: 106443, doi: 10.1016/j.ecss.2019.106443

Charnock H. 1955. Wind stress on a water surface. Quarterly Journal of the Royal Meteorological Society, 81(350): 639–640, doi: 10.1002/qj.49708135027

Craig P D, Banner M L. 1994. Modeling wave-enhanced turbulence in the ocean surface layer. Journal of Physical Oceanography, 24(12): 2546–2559, doi: 10.1175/1520-0485(1994)024<2546:MWETIT>2.0.CO;2

Deng Zengan, Zhao Yifei. 2020. Impact of tidal mixing on water mass properties and circulation in the Bohai Sea: a typhoon case. Journal of Marine Systems, 206: 103338, doi: 10.1016/j.jmarsys.2020.103338

Denman K L, Miyake M. 1973. Upper layer modification at ocean station *Papa*: observations and simulation. Journal of Physical Oceanography, 3(2): 185–196, doi: 10.1175/1520-0485(1973)003<0185:ULMAOS>2.0.CO;2

Donelan M A. 1990. Air-sea interaction. In: Le Mehaute B, Hanes D M, eds. The Sea: Ocean Engineering Science. New York: Wiley-Interscience Press, 239–292

Drennan W M, Kahma K K, Terray E A, et al. 1992. Observations of the enhancement of kinetic energy dissipation beneath breaking wind waves. In: Banner M L, Grimshaw R H J, eds. Breaking Waves: IUTAM Symposium Sydney, Australia 1991. Berlin, Heidelberg: Springer, 95–101

Drennan W M, Taylor P K, Yelland M J. 2005. Parameterizing the sea surface roughness. Journal of Physical Oceanography, 35(5): 835–848, doi: 10.1175/JPO2704.1

Feddersen F. 2012. Observations of the surf-zone turbulent dissipation rate. Journal of Physical Oceanography, 42(3): 386–399, doi: 10.1175/JPO-D-11-082.1

Gao Shuanzhu, Meng Zhiyong, Yang Guiming. 2009. Study on the predictability of the recurvature of Typhoon Matsa (0509) in Bohai. Meteorological Monthly, 35(2): 8–14

Gaspar P. 1988. Modeling the seasonal cycle of the upper ocean. Journal of Physical Oceanography, 18(2): 161–180, doi: 10.1175/1520-0485(1988)018<0161:MTSCOT>2.0.CO;2

Gemmrich J R, Farmer D M. 1999. Near-surface turbulence and thermal structure in a wind-driven sea. Journal of Physical Oceanography, 29(9): 480–499, doi: 10.1175/1520-0485(1999)029<0480:NSTATS>2.0.CO;2

Gerbi G P, Trowbridge J H, Terray E A, et al. 2009. Observations of turbulence in the ocean surface boundary layer: energetics and transport. Journal of Physical Oceanography, 39(5): 1077–1096, doi: 10.1175/2008JPO4044.1

Ginis I. 2002. Tropical cyclone-ocean interactions. In: Perrie W, ed. Atmosphere-Ocean Interactions. Southampton: WIT Press

Han Guijun, Li Wei, He Zhongjie, et al. 2006. Assimilated tidal results of tide gauge and TOPEX/POSEIDON data over the China seas using a variational adjoint approach with an onlinear numerical model. Advances in Atmospheric Sciences, 23(3): 449–460

Janssen P A E M. 2001. Reply. Journal of Physical Oceanography, 31(8): 2537–2544, doi: 10.1175/1520-0485(2001)031<2537:R>2.0.CO;2

Jones N L, Monismith S G. 2008. Modeling the influence of wave-enhanced turbulence in a shallow tide- and wind-driven water column. Journal of Geophysical Research, 113(C3): C03009, doi: 10.1029/2007JC004246

Kraus E B, Turner J S. 1967. A one-dimensional model of the seasonal thermocline II. The general theory and its consequences. Tellus, 19(1): 98–106, doi: 10.3402/tellusa.v19i1.9753

Liu Jiajun, Zhang Lifeng, Guan Jiping, et al. 2010. Application of ensemble prediction products to the forecast of Typhoon Masta. Meteorological Monthly, 36(5): 21–31

Mellor G L. 2001. One-dimensional, ocean surface layer modeling: a problem and a solution. Journal of Physical Oceanography, 31(3): 790–809, doi: 10.1175/1520-0485(2001)031<0790:ODOSLM>2.0.CO;2

Mellor G, Blumberg A. 2004. Wave breaking and ocean surface layer thermal response. Journal of Physical Oceanography, 34(3): 693–698, doi: 10.1175/2517.1

Mellor G L, Durbin P A. 1975. The structure and dynamics of the ocean surface mixed layer. Journal of Physical Oceanography, 5(4): 718–728, doi: 10.1175/1520-0485(1975)005<0718:TSADOT>2.0.CO;2

Mellor G L, Yamada T. 1974. A hierarchy of turbulence closure models for planetary boundary layers. Journal of the Atmospheric Sciences, 31(7): 1791–1806, doi: 10.1175/1520-0469(1974)031<1791:AHOTCM>2.0.CO;2

Mellor G L, Yamada T. 1982. Development of a turbulence closure model for geophysical fluid problems. Reviews of Geophysics, 20(4): 851–875, doi: 10.1029/RG020i004p00851

Meng Qingjun, Li Peiliang, Zhai Fangguo, et al. 2020. The vertical mixing induced by winds and tides over the Yellow Sea in summer: a numerical study in 2012. Ocean Dynamics, 70(7): 847–861, doi: 10.1007/s10236-020-01368-2

Phillips O M. 1977. Dynamtics of the Upper Ocean. Cambridgeshire: Cambridge University Press, 366

Polton J A, Lewis D M, Belcher S E. 2003. The Role of Wave-Induced Coriolis-Stokes Forcing on the Wind-Driven Mixed Layer. Journal of Physical Oceanography, 35(4): 444–457

Ren Huiru, Li Guosheng, Cui Linlin, et al. 2016. Wave climate changes in Bohai Sea related to the East Asian circulation oscillations over the last sixty years. Climatic and Environmental Research, 21(4): 490–502, doi: 10.3878/j.issn.1006-9585.2016.15281

Scully M E, Trowbridge J H, Fisher A W. 2016. Observations of the transfer of energy and momentum to the oceanic surface boundary layer beneath breaking waves. Journal of Physical Oceanography, 46(6): 1823–1837, doi: 10.1175/JPO-D-15-0165.1

Shao Jinchao, Zhao Hui, Shen Chunyan, et al. 2015. Influence of typhoon Matsa on phytoplankton Chlorophyll-a in the Northwest Pacific Ocean offshore and alongshore. Journal of Guangdong Ocean University, 35(4): 67–74

Smith S D, Anderson R J, Oost W A, et al. 1992. Sea surface wind stress and drag coefficients: the hexos results. Boundary-Layer Meteorology, 60(1–2): 109–142, doi: 10.1007/BF00122064

Song Wenpeng. 2009. The analysis of the structure of T-S and the current characteristics in Baohai Sea during winter and summer (in Chinese)[dissertation]. Qingdao: Ocean University of China

Song Yaoling. 2012. Effect of activity characteristics of Typhoon Matsa on aviation meteorological observation and support. Meteorological, Hydrological and Marine Instruments (in Chinese), 29(1): 99–104, doi: 10.3969/j.issn.1006-009X.2012.01.026

Stacey M W. 1999. Simulation of the wind-forced near-surface circulation in Knight Inlet: a parameterization of the roughness length. Journal of Physical Oceanography, 29(6): 1363–1367, doi: 10.1175/1520-0485(1999)029<1363:SOTWFN>2.0.CO;2

Sun Qun, Guan Changlong, Song Jinbao. 2006. Effect of wave breaking on turbulent energy budgets in ocean surface mixed layer.

Oceanologia et Limnologia Sinica, 37(1): 69–74, doi: 10.3321/j.issn:0029-814X.2006.01.011

Terray E A, Donelan M A, Agrawal Y C, et al. 1996. Estimates of kinetic energy dissipation under breaking waves. Journal of Physical Oceanography, 26(5): 792–807, doi: 10.1175/1520-0485(1996)026<0792:EOKEDU>2.0.CO;2

Terray E A, Donelan M A, Agrawal Y C, et al. 1997. Reply. Journal of Physical Oceanography, 27(10): 2308–2309, doi: 10.1175/1520-0485(1997)027<2308:R>2.0.CO;2

Terray E A, Drennan W M, Donelan M A. 1999. The vertical structure of shear and dissipation in the ocean surface layer. In: Proceedings of Symposium on the Wind-driven Air-Sea Interface—Electromagnetic and Acoustic Sensing, Wave Dynamics, and Turbulent Fluxes. Sydney: University of New South Wales, 239–245

Toba Y, Smith S D, Ebuchi N. 2001. Historical drag expressions. In: Jones I S F, Toba Y, eds. Wind Stress over the Ocean. New York: Cambridge University Press

Wunsch C, Ferrari R. 2004. Vertical mixing, energy, and the general circulation of the oceans. Annual Review of Fluid Mechanics, 36: 281–314, doi: 10.1146/annurev.fluid.36.050802.122121

Yablonsky R M, Ginis I. 2008. Improving the ocean initialization of coupled hurricane–ocean models using feature-based data assimilation. Monthly Weather Review, 136(7): 2592–2607, doi: 10.1175/2007MWR2166.1

Yang Yongzeng, Qiao Fangli, Xia Changyong, et al. 2003. Effect of ocean wave momenfum and mixing on upper ocean. Advances in Marine Science, 21(4): 363–368, doi: 10.3969/j.issn.1671-6647.2003.04.001

Zhang Xuefeng, Han Guijun, Wu Xinrong, et al. 2011. Effect of surface wave breaking on upper-ocean structure revealed by assimilating sea temperature data. Journal of Tropical Oceanography, 30(5): 48–54, doi: 10.11978/j.issn.1009-5470.2011.05.048

Zhao Yifei, Deng Zengan, Yu Ting, et al. 2019. Numerical study on tidal mixing in the Bohai Sea. Marine Geodesy, 42(1): 46–63, doi: 10.1080/01490419.2018.1539055

Zhao Xin, Sun Qun. 2013. Influence of reclamation on hydrodynamic environment in Bohai Bay. Advanced Materials Research, 726–731: 3262–3265, doi: 10.4028/www.scientific.net/AMR.726-731.3262

Zippel S F, Thomson J, Farquharson G. 2018. Turbulence from breaking surface waves at a river mouth. Journal of Physical Oceanography, 48(2): 435–453, doi: 10.1175/JPO-D-17-0122.1